Advances in Magnetics

Micro-Brillouin Light Scattering Spectroscopy of Magnetic Nanostructures

Sergej O. Demokritov and Vladislav E. Demidov

Institute of Applied Physics, Münster University, Münster 48149, Germany

We describe a new technique, micro-Brillouin light scattering spectroscopy, for investigation of spin wave dynamics in magnetic nanostructures. The technique offers advantages for studies of small magnetic squares with closure domain structure and magnetic nanoelements similar to those used in magnetic random access memory. The technique is particularly effective in two-dimensional mapping of spin waves excited by a single nanocontact due to the spin torque transfer effect.

Index Terms—**Brillouin scattering, magnetic nanostructured materials, spin waves.**

I. INTRODUCTION

RECENT development of magnetic random access memory elements as a new generation of fast nonvolatile electronic memory and magnetic read heads for hard disk drives with an ultimate storage density has brought high attention of scientists and engineers to magnetic nanostructures [1], [2]. The main directions in the development of magnetic memory are the growth of the integration level and the increase of the operating speed. Since the data rate in magnetic memory devices has reached the gigahertz range and switching time is pushed well into the gyromagnetic regime, precessional dynamic magnetization processes in nanoelements came into focus of interest in the last years (see, e.g., [3]–[25] and references therein). On the other hand, the size of those nanoelements is still above the single-domain limit. Therefore, the magnetic dynamics in those elements is mainly determined by nonuniform magnetic eigen-excitations. The same excitations cause the high-frequency magnetic thermal noise existing in the elements, which limits the figure of merit of magnetic memory elements and reading heads. In unconfined magnetic systems magnetic excitations are described by plane spin waves, whereas in nanoelements confined spin-wave modes should be considered. Basic knowledge on spin-wave modes is mandatory to understand dynamic processes in magnetic nanostructures.

A technique for investigation of nonuniform spin-wave modes in magnetic nanostructures should combine a submicrometer spatial resolution with subnanosecond temporal resolution. Brillouin light scattering (BLS) spectroscopy [4], [14], [20], [23], [26] fulfills the above requirements. As alternatives to BLS, several techniques can be considered. Time-resolved Kerr-microscopy is widely used for investigation of magnetic dynamics [6], [9], [10], [13], [17], [19], [20]. Using the pump-probe approach, one can stroboscopically investigate magnetic dynamics excited either by a pulse of magnetic field or by a short laser pulse. The magnetic response of the system is then probed by another laser pulse and recorded as a function of the delay time between the pump and the probe. The information on spin-wave modes can be extracted from the measured temporal dependence using following Fourier analysis. To detect spin-wave frequencies of 10 GHz, one should record the response of the systems with the temporal resolution below 50 ps. On the other hand, the frequency resolution in this approach is determined by the interval of the recorded delay times. To obtain the resolution below 0.1 GHz, delay times above 10 ns are needed. A disadvantage of the Kerr-microscopy is its relatively low sensitivity in comparison with BLS: up to now, rather strong excitation pulses are needed to excite a detectable response of the system.

X-ray microscopy [18] promises a very high spatial (below 20 nm) resolution. However, it is not well suited for the observation of high-frequency magnetization oscillations due to its relatively poor temporal resolution [25].

BLS spectroscopy is a very sensitive technique, which allows for investigations of inhomogeneous magnetization dynamics [26]. It has numerous advantages over the above techniques: 1) spin-wave modes with very high frequencies up to 500 GHz can be detected; 2) since the data are analyzed in the frequency domain, an ultimate frequency resolution down to 50 MHz can be obtained; 3) extremely high sensitivity of BLS allows for detection of thermally excited spin waves, i.e., there is no need for external excitation sources. However, up to recently, the application of BLS for studies of nanostructures was restricted by its poor lateral resolution defined by the size of the probing laser spot, which was usually 30–40 μm in diameter. The invention of micro-BLS [23], where the laser beam is focused almost down to the theoretical diffraction limit of 200–250 nm and the scattered light can be effectively collected from this small area for further spectral analysis, has opened new perspectives for BLS. Magnetic dynamics of single elements with submicrometer sizes is accessible now [14], [23]. Such interesting phenomena as spin-wave radiation by nanocontacts due to the spin-torque transfer effect can be studied directly and two-dimensional (2-D) maps of the excited spin waves can be recorded [4]. Dynamic coupling between magnetic nanoelements due to radiation of spin waves by quantized spin-wave modes within the element should be mentioned as well [5].
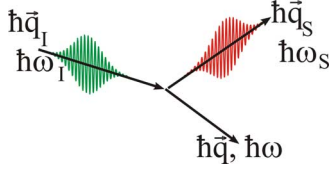
Fig. 1. Inelastic BLS process. An incident photon creates a magnon and as a consequence loses its energy. The change of the photon energy is equal to the energy of the created magnon.

Application of micro-BLS for investigation of spin waves and spin-wave modes in magnetic nanostructures is the subject of this paper.

II. BRILLOUIN LIGHT SCATTERING (BLS) TECHNIQUE

A. BLS-Process and Conservation Laws

Inelastic Brillouin light scattering [26] is a spectroscopic method for investigations of excitations with frequencies from 1 to 500 GHz. Magnons, which are elementary quanta of spin waves, contribute to the BLS-process in magnetic media. By detecting this contribution using a spectroscopic device, one can obtain valuable information on the excitations.

As illustrated in Fig. 1, a photon of energy $\hbar\omega_I$ and momentum $\hbar\vec{q}_I$ propagating in a magnetic medium creates a magnon ($\hbar\omega$, $\hbar\vec{q}$). The scattered photon possesses a smaller energy and different momentum

$$\hbar\omega_S = \hbar(\omega_I - \omega), \quad \hbar\vec{q}_S = \hbar(\vec{q}_I - \vec{q}). \tag{1}$$

A magnon can also be absorbed during a similar process. In this case, the energy of the scattered photon is larger than that of the incident one. For room temperature $T_R \gg \hbar\omega/k_B \approx 0.1 - 10$ K, both processes have about the same probability. From (1), it is evident that the wave vector $\vec{q}_I - \vec{q}_S$, transferred in the scattering process, is equal to the wave vector $\vec{q}$ of the spin wave. Thus, choosing the scattering geometry, one can select the direction and the absolute value of the wave vector of the magnon, participating in the scattering process. From the analysis of the scattered light, the frequency of the magnon can be determined, provided the incident light is monochromatic. The electromagnetic field of the scattered wave is proportional to the product of the magneto-optical constants of the medium and the amplitude of the dynamic magnetization, corresponding to the spin wave. Thus, the BLS intensity, determined by the squared field, is directly proportional to the dynamic magnetization squared. Magneto-optical effects relate the dielectric tensor of the medium with Cartesian components of its magnetization. Usually the nondiagonal elements of the tensor, the magneto-optical effects (magnetic birefringence and the Faraday effect) are responsible for the scattering. Therefore, the plane of polarization of the scattered light is rotated by 90° with respect to that of the incident light.

The conservation laws, given by (1), follow from the time invariance of the problem and the translation invariance of an infinite medium, correspondingly. However, if the scattering volume is finite, the selection rule for the momentum is broken. For the scattering volume with a size less or comparable with the
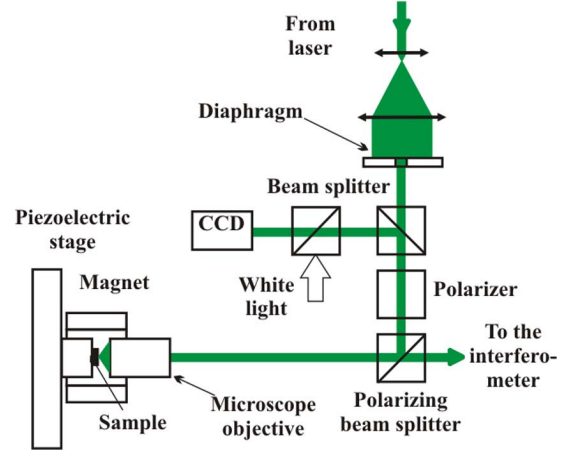

Fig. 2. Micro-BLS setup. Elements of the setup are described in the main text.

wavelength of the light, any magnon with a wave vector comparable with that of light contributes to the scattering process. The confinement of the scattering volume can come from the finite size of the element under consideration and/or from a small diameter of the focused laser beam. This is in particular important in the case of the micro-BLS technique.

B. Micro-BLS Setup

The setup for micro-BLS measurements is shown in Fig. 2. A laser beam is typically used as a source of monochromatic incident light. To obtain a small focal spot of the incident beam, it is of great importance to apply a laser beam corresponding to a single spatial mode and to reduce the divergence of the beam. For this purpose, the primary beam is expanded by means of a beam expander and spatially filtered using a small round diaphragm. Note, that a pin-hole arrangement can be used for the same purposes. The resulting beam of the TEM_{00} spatial mode is transmitted through a thin-film polarizer increasing the vertical polarization degree of up to 10^4. Such a high polarization degree of the incident beam improves the figure of merit of the coarse filtering of the inelastically scattered light from the elastically scattered (reflected) one, based on their orthogonal polarization planes. Then the beam is reflected by a polarizing beam splitter and focused by a microscope objective onto the surface of the sample placed into a magnetic field. The objective is characterized by a high magnification (100×) and a large numerical aperture (0.75). It allows for a focusing of TEM_{00} beams with small divergences down to about 250 nm and an effective collection of the scattered light from this tiny area for further spectral analysis. To avoid overheating of the sample by the focused laser beam, the laser power does not usually exceed 5–10 mW. The sample is mounted on an xyz piezoelectric stage, which provides the sample positioning along all three dimensions with a precision of about 50 nm.

The probing light is inelastically scattered by spin waves resulting in changes of the light frequency. To detect the inelastically scattered light the spectrum of the scattered light is analyzed by means of a tandem Fabry–Pérot interferometer operating in multipass configuration. The frequency resolution of the interferometer allows for the detection of magnons with frequencies down to 1 GHz. As mentioned above, a coarse separation of the weak inelastically scattered light from the very
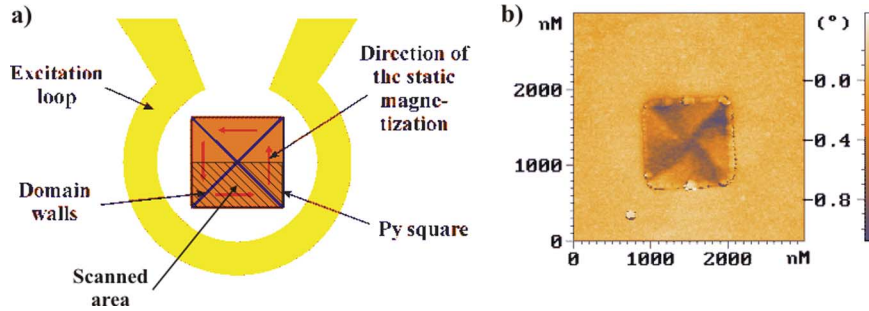
Fig. 3. (a) Schematic layout of a sample: a magnetic permalloy square is placed in an excitation loop. The solid lines show the domain walls, whereas the arrows indicate the directions of the static magnetization in each domain. The shadowed area has been imaged using BLS. (b) Image of the domain structure of a magnetic square made by means of magnetic force microscopy.

intensive light reflected from the sample surface is performed using a polarizing beam splitter, which transmits the horizontally polarized scattered light and suppresses the vertically polarized component in the transmitted light by a factor of 10^4. This separation provides a reasonable signal-to-noise ratio for the following analysis using the Fabry–Pérot interferometer.

Taking into account the value of the numerical aperture of the objective and the uncertainty in the wave vector of the scattered light caused by the spatial confinement, the micro-BLS setup does not provide any wave vector selectivity. Instead the contributions from all spin waves up to a certain wave vector are automatically integrated. One can easily estimate the cutoff wave vector, limiting the sensitivity of the setup: $q_{max} \approx (1.5 - 2.5) \times 10^5$ cm^{-1}, depending on the wavelength of the laser beam. Thus, one can simultaneously collect a BLS signal from all spin waves propagating in different directions and having their wave vectors $|q| \leq q_{max}$.

For investigation of magnetic nanostructures, it is extremely important to place the laser spot on the appropriate element of the structure and to keep it at the same place over the measurement time. For a visual control of the position of the laser spot on the surface of the sample, a viewing system is integrated into the setup. This system consists of a CCD camera supplied with a telescopic objective, two beam splitters, and a source of white light (see Fig. 2). The system allows for the direct observation of the surface of the sample and the position of the probing laser spot on the screen of a monitor during measurements. In extreme cases an active beam stabilization technique, based on a digital analysis of the obtained image and linked with the piezoelectric stage, can be applied.

The described setup can also be used for investigation of nonmagnetic systems. Recently, a study of single isolated silica sphere of diameter as small as 260 nm has been reported [27].

III. PERMALLOY SQUARES WITH CLOSURE DOMAIN STRUCTURE

In the last decade, confined spin-wave modes of micrometer-sized magnetic elements have been systematically studied for the straightforward case of elements possessing an almost monodomain state [8], [10], [16], [21], [22], [24]. Significantly less is known about magnetization dynamics in magnetic nanostructures brought to a multidomain state, characterized by inhomogeneous distributions of the static magnetization. A magnetic disk in the vortex state characterized by an axial symmetry is one example of such a system. Confined spin-wave modes of magnetic nanodisk with vortex structure is now intensively studied

both theoretically and experimentally [9], [17], [19], [22] and seems to be well understood. Another example of such a system is a square in the flux closure Landau state, obeying the four-fold symmetry. Although such a state has been known for almost 70 years [28], a theoretical description of its spin-wave mode spectrum has appeared only recently [11], [12]. This is mainly due to complexity of the problem caused by abrupt rotation of the magnetization at domain walls between the four domains which introduces drastic changes in the magnetic energy landscape.

Micro-BLS technique has been used for investigation of the spin-wave spectra of micrometer- and submicrometer-sized $Ni_{80}Fe_{20}$ squares with Landau domain structure. Each studied sample represents a single, ferromagnetic $Ni_{80}Fe_{20}$ square with a lateral size ranging from 0.75 to 4 μm. The samples were produced by e-beam evaporation on a Si substrate and capped with 2 nm Al for corrosion protection. The square was placed inside a single turn Au loop of 300 nm thickness connected to a 50 Ω microstrip transmission line. The loop has inner and outer diameters of 8 and 12 μm, respectively, as shown in Fig. 3(a). The sample thickness, d and its saturation magnetization, $4\pi M_s$ were 16 nm and 10.1 kG, respectively. Before the measurements the samples were demagnetized using a gradually decreasing ac magnetic field applied perpendicularly to the plane of the samples. The existence of a four-fold closure domain structure was proven for every sample by means of magnetic force microscopy [see Fig. 3(b)].

First, spectra of quantized spin waves existing in the samples due to thermal fluctuations were studied, as shown in Fig. 4. The four spectra correspond to squares with lateral dimensions of (a) 0.75 μm, (b) 1 μm, (c) 2 μm, and (d) 4 μm. The accumulation time of each spectrum was 2 h. The spectra were analyzed in the frequency range from 2 to 14 GHz. The probing laser spot was positioned in the middle of one of the four triangular domains of the closure domain structure. The lower frequency limit (2 GHz) was determined by the influence of the elastically scattered light, nonfiltered by the Brillouin spectrometer due to its finite finesse.

As seen from Fig. 4, up to six peaks can be clearly distinguished in the spectrum corresponding to the square with the minimum size of 0.75 μm. With increasing size of the square, the frequencies corresponding to the peaks decrease and the spectrum becomes denser. In addition to the decreasing distance between the lines corresponding to different spin-wave modes, an increasing linewidth of each individual line should be mentioned. In fact, the finite decay length of spin waves which can be estimated in our samples as 1–2 μm becomes more and more important for the linewidth of the modes with increasing size
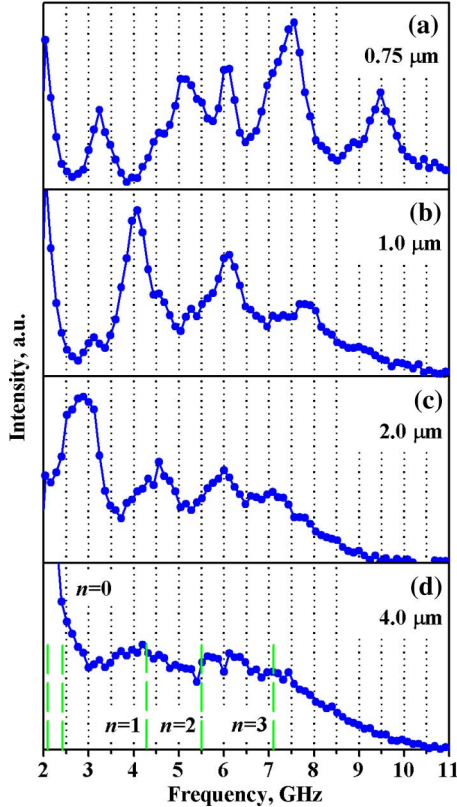
Fig. 4. Spectra of thermal spin waves for the squares with dimensions of (a) 0.75 μm, (b) 1 μm, (c) 2 μm, and (d) 4 μm. Dashed lines in the part (d) indicate the frequencies corresponding to the distributions of the dynamic magnetization presented in Fig. 5.
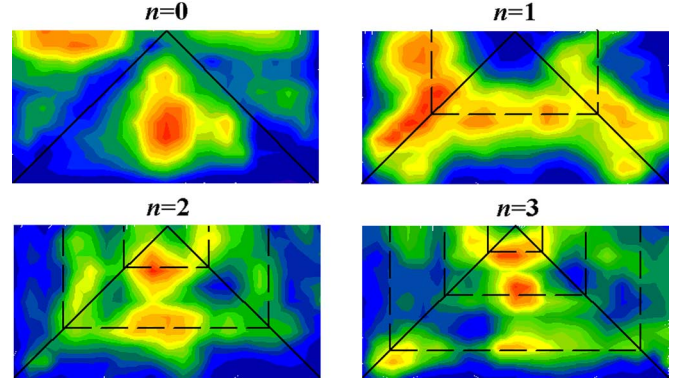

Fig. 5. Distributions of the amplitude of dynamic magnetization corresponding to the eigenmodes at different frequencies. Diagonal solid lines indicate the domain walls. The corresponding quantization numbers n are indicated near the distributions.
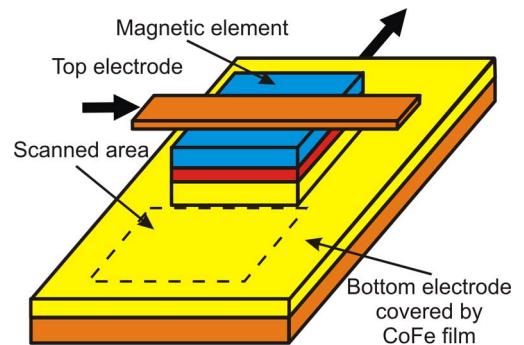

Fig. 6. Schematic view of a magnetic element with partially patterned bottom magnetic layer. The bold arrows indicate the direction of the electric current.

of the square. As a result, the square with lateral dimensions of $4 \mu m$ becomes weakly resonant, the spectrum comprising several broad, strongly overlapping peaks.

In order to classify the detected eigenmodes space resolved measurements were performed, allowing for the imaging of lateral distributions of the dynamic magnetization. For this purpose, the largest (4 μm) square was chosen as giving the maximum dynamic interval for spatial measurements. Since the frequencies of the eigenmodes of such a square were not clearly resolved, micro-BLS imaging was performed for frequencies in the range from 2 to 8 GHz with a frequency step of 100 MHz. In order to improve the sensitivity and to filter modes with fast spatial changes, an external excitation field at a fixed frequency was applied to the samples by means of transmission of a monochromatic microwave current through the excitation loop. The probing laser spot was scanned in two dimensions with a step size of 200 nm. Since BLS imaging with a high spatial resolution is very time consuming, and taking into account the four-fold symmetry of the system being investigated, only half of the square was scanned as shown in Fig. 3(a). The measured distributions of dynamic magnetization are presented in Fig. 5. As seen from Fig. 5, profiles obtained by means of the space-resolved BLS-measurements are spread over the entire domain and clearly show quantization behavior. They can unambiguously be labeled by the number n of antinodes of the amplitude of the dynamic magnetization along a direction from the center of the square to its edges, i.e., along the direction perpendicular to the static magnetization in the domain. The mode shown in Fig. 5(a) has no antinodes, (b) has one antinode

along this direction, (c) has two antinodes, and (d) three antinodes. Consequently, we label these modes with a transversal quantization number n equal to 0, 1, 2, and 3, respectively.

Similar to the spin-wave modes observed in magnetically saturated stripes [29] the frequencies of the modes increase with increasing quantization number. This fact can be qualitatively explained using a dispersion law for plane spin waves of an unconfined film, magnetically saturated in its plane [30]. In fact, the frequency of spin waves with their wave vector oriented perpendicularly to the static magnetization increases with increasing wave vector. Consequently, a standing spin wave with larger number of anti-nodes (larger effective wave vector) along the direction perpendicular to the static magnetization should have higher frequency.

IV. RECTANGULAR SPIN-VALVE MEMORY ELEMENT: SPIN-WAVE QUANTIZATION AND RADIATION

The strong potential of MRAM technology for the creation of a new nonvolatile electronic memory is the potential growth of not only the integration level and the extreme data safety, but the increase of the operating speed as well. Therefore, fast magnetization dynamics of MRAM elements is of particular interest. Spin wave modes have been investigated in a sample of geometry typical for MRAM. The layout of a sample is shown in Fig. 6.

The magnetic multilayer element 2 nm Au/5 nm $Ni_{80}Fe_{20}$/ 4 nm Cu/10 nm $Co_{80}Fe_{20}$ with lateral dimensions of $a \times b = 1.3 \times 2.3 \ \mu m^2$ is fabricated between the top and the bottom electrodes by means of optical lithography and following ion
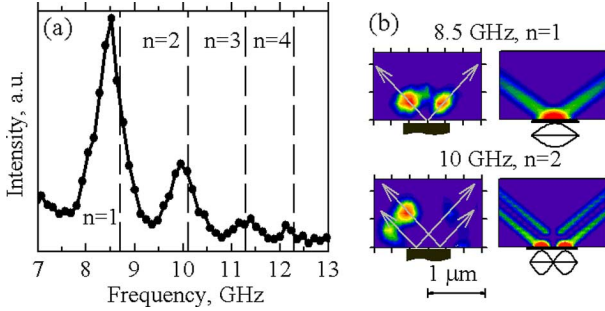
Fig. 7. (a) Spectrum of quantized spin wave modes of the magnetic element measured with the probing laser spot positioned onto the open part of the element. The modes are excited by the microwave current; (b) experimental (left column) and simulated (right column) 2-D maps of the spin waves radiated by the two lowest modes outside the element. The arrows show directions of radiated rays in accordance with the theoretical results.

milling. The milling was stopped in the CoFe layer providing a 5–6 nm thick $Co_{80}Fe_{20}$ film, which surrounds the element. This film was used for detection of spin waves radiated by the element. A transparent insulating Al_2O_3 layer allows for the optical access to this area and the part of the element which is not covered by the upper electrode. For spin wave excitation, a microwave current flowing through the element and crossing all magnetic layers has been used. The frequency of the exciting current was continuously swept from 7.5 to 13 GHz.

To detect the spectrum of the spin waves existing in the element [see Fig. 7(a)], the probing laser spot is positioned onto the magnetic element.

As seen from the figure, spin waves in the element demonstrate strong quantization corroborated by appearance of several well-pronounced peaks in the spectrum. In order to identify the peaks the frequencies of quantized spin-wave eigenmodes of the element were calculated using the known dispersion law for spin waves in a film [30] and the pinned boundary condition for the dynamic magnetization at the edges of a magnetic element [31]. This condition corresponds to the quantization for the spin-wave wave vector $q^2 = (n\pi/a)^2 + (m\pi/b)^2$, where $n, m = 1, 2 \ldots$ The calculation shows that the observed peaks correspond to spin-wave modes quantized in the direction perpendicular to the static magnetization, i.e., $n = 1, 2, 3, 4$ and $m = 1$. The frequencies of these eigenmodes shown in Fig. 7(a) by the dashed lines agree well with the positions of the measured peaks.

If, however, the probing laser spot is positioned onto the unconfined surrounding film, spin waves radiated by the element are detected. It has been found that these spectra also exhibit peaks at frequencies corresponding to those of the quantized eigenmodes of the element. Two-dimensional distributions of the BLS-intensity for the two lowest-order modes are shown in the left column of Fig. 7(b). They are obtained by scanning the laser focus across the area shown in Fig. 6 and keeping the excitation frequency equal to one or another resonance value, as indicated near each pattern. The patterns demonstrate several spots where the spin-wave intensity significantly increases, but the positions and the numbers of these spots are different for different radiating eigenmodes. In order to understand the observed radiation patterns calculations were performed. The amplitude of the dynamic magnetization in every point of the con-

tinuous film was calculated taking into account the interference of spin waves coming from different parts of the element. Magnetic dissipation was neglected. The results of the calculations are presented in the right column of Fig. 7(b), allowing a qualitative understanding of the experimental findings. If the radiating mode $(n = 1)$ has a distribution with one anti-node, spin waves are radiated in two rays starting at the point where the distribution has its maximum. If the distribution has two anti-nodes $(n = 2)$, the number of rays increases to four. In this case, on the middle line, where the rays intersect each other, a complete suppression of the dynamic magnetization is observed caused by the destructive interference. Thus, the presented study using the micro-BLS setup demonstrates that 2-D radiation of spin waves by a magnetic element is determined by the quantized eigenmodes of the elements. The radiation patterns consist of several rays interfering one with the other and forming spots where the intensity of dynamic magnetization locally increases. The number of rays and the spots as well as their positions in space depends on the order of the radiating eigenmodes.

V. SPIN-VALVE NANOCONTACT: SPIN-WAVE AMPLIFICATION BY DIRECT SPIN-POLARIZED ELECTRIC CURRENT

Spin-wave excitation by a spin-polarized direct electric current flowing through a multilayer has been predicted theoretically [32] and later observed experimentally [33] in nanopillars and nanocontacts. Recently, this phenomenon has attracted enormous attention due to its potential for nanometer-scale microwave oscillators to be used in future integrated microelectronic devices (see, e.g., [33]–[37] and references therein). It is now well established that the spin-polarized current exerts a torque on the magnetization of a ferromagnetic layer (the spin-torque-transfer effect), which leads to modification of the damping constant of the medium and to the excitation of microwave-frequency magnetic precession and the generation of spin waves if the current strength and its degree of polarization are high enough for the damping constant to change its sign. Here, we illustrate the ability of the micro-BLS technique for investigation of the effect of spin-polarized direct electric current on spin-wave radiation [38].

The sample under study is very similar to that shown in Fig. 6. Since a high current density is necessary for the spin-torque-transfer effect, the size of the element is further reduced to 300×300 nm^2. In addition, the stack is inversed with respect to the sample discussed in the previous subsection: $Ni_{80}Fe_{20}$ forms a film surrounding the element. In the same way as described in the previous subsection, the radiation of spin waves excited by a microwave current flowing through the element is analyzed. The spectrum of the quantized eigenmodes and 2-D maps of the radiated spin waves are shown in Fig. 8(a) and (b), respectively.

The spectrum presented in Fig. 8(a) clearly shows two quantized eigenmodes at 4.3 and 5.4 GHz, corresponding to $n = 1$ and $n = 2$. Fig. 8(b) presents 2-D distributions of the intensity of spin waves radiated from the element by each mode. The distributions were recorded with the exciting current being kept at a fixed frequency of 4.3 and 5.4 GHz, respectively. The difference in the detected intensities for two modes is connected with different wave vectors of the radiated waves. In fact, the higher-order mode radiates spin waves with larger wave vectors. The considered spin waves with the wave vector parallel
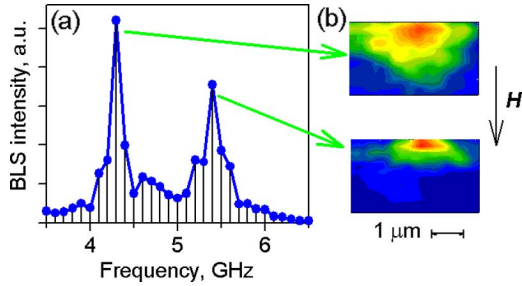
Fig. 8. (a) Spectrum of quantized spin wave modes of the magnetic nanocontact excited by the microwave current. The probing laser spot is positioned close to the contact; (b) experimentally recorded 2-D maps of the spin waves radiated by the two modes outside the contact.
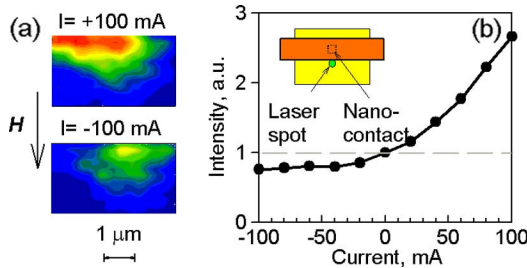

Fig. 9. (a) Influence of a direct current on the intensity of radiated spin waves. Color scales are the same as in Fig. 8(b). (b) Dependence of the local intensity of radiated spin waves on the strength of the direct current. Inset—geometry of the local measurements.

to the static magnetization correspond to the geometry of the so-called backward volume spin waves [30]. For this geometry, the group velocity decreases with increasing wave vector for the wave vector interval where the magnetic dipole interaction dominates. Thus, the decay length is smaller for higher modes, even if the damping time, determined by the effective Gilbert damping, is the same for both spin wave modes. Due to a smaller size of the element the interference effects of the radiated spin waves are negligible; therefore, the spin waves are radiated almost axially symmetrically.

The influence of a spin-polarized direct current on the spin-wave radiation process is illustrated in Fig. 9.

The microwave current of constant amplitude at the frequency of the lowest mode, i.e., 4.3 GHz, was applied to the element. In addition to the microwave current, a direct current varied in the range of -100 mA to 100 mA (current density up to 10^8 A/cm^2) has been passed through the contact. The obtained 2-D maps of the measured spin-wave intensity similar to those presented in Fig. 8(b) are shown in Fig. 9(a) for both a positive and a negative direct current. The positive direction of the current is associated with the electrons flowing from the continuous Ni$_{80}$Fe$_{20}$ film to the patterned element. As seen from the figure, a positive current of 100 mA leads to a noticeable increase of the intensity of radiated spin waves, whereas transmission of a negative current of -100 mA leads to a decrease of the spin-wave intensity.

The observed influence of the direct current on the intensity of radiated spin waves can be understood by the spin-torque applied to the magnetization of the Ni$_{80}$Fe$_{20}$ layer by the spin-polarized current. In fact, due to the spin-torque effect the effective damping of magnetic precession in the element is affected by the spin-polarized current in such a way that for one direction of the current the effective damping of the precession decreases, whereas for another direction it increases. Since the

damping determines the value of the high-frequency susceptibility of the medium, the amplitude of the eigenmodes in the element excited by the microwave current is increased or reduced depending on the direction of the current. Further quantitative information about the influence of the spin-polarized current on the intensity of radiated spin waves is given in Fig. 9(b). The figure shows the local spin-wave intensity at a given point as a function of the direct current. The shown intensity is normalized to the intensity obtained without direct current. As seen from the figure, the transmission of a positive electric current leads to a strong increase of the spin-wave intensity more than by a factor of two for the current rising up to 100 mA. As a negative current is applied the intensity starts gradually to decrease with the rate, which is much smaller than that for the case of spin-wave amplification at positive currents.

To analyze this effect, one should take into account that the spin-torque-transfer effect is essential in the nanocontact area only. Therefore, the direct current affects the spin wave excitation in the nanocontact, but not its propagation in the Ni$_{80}$Fe$_{20}$ film. Let us further imply that the microwave current creates a high-frequency field h. The dynamic magnetization in the nanocontact is then connected with h through the high-frequency susceptibility χ (see, e.g., [39]):

$$\chi \approx \frac{i\omega\omega_M}{\Omega^2 - (\omega + i\alpha\Omega)^2}. \quad (2)$$

Here, ω and Ω are the frequency of the exciting field and the resonant frequency, respectively. $\alpha \ll 1$ is the effective damping constant describing both the Gilbert damping and the spin-torque-transfer effect. Finally, $\omega_M = 4\pi\gamma M$, where γ is the gyromagnetic ratio and M is the static magnetization of the film. Taking into account the resonance condition $\omega = \Omega$, one obtains

$$m = \chi h \approx \frac{\omega_M}{2\alpha\Omega}h \propto \frac{1}{\alpha}. \quad (3)$$

Thus, the BLS-intensity, which is proportional to the dynamic magnetization squared, should follow to $1/\alpha^2$, if α is modified by the direct current. This fact is illustrated in Fig. 10, where inverse square root of the BLS-intensity ($\propto \alpha$) is plotted as a function of the direct current.

For positive values of the direct current Fig. 10 clearly demonstrates a linear decrease of the effective damping constant due to the spin-torque-transfer effect, predicted in [31] and experimentally observed in [34]. One can also conclude that the critical current of about 250 mA should be applied to realize a spontaneous excitation of spin waves just by a direct current, without any microwave current.

Surprisingly, this linear dependence breaks down for negative values of the direct current beyond 20 mA. Up to now it is not clear whether this observation demonstrates a discrepancy between the experiment and the theory or it is connected with a simplified analysis of the problem based on (2). In fact, there are several quantized spin-wave eigenmodes in the nanocontact. With increasing effective damping of the resonant mode excited by the microwave current, the effect of off-resonant excitation of other modes can play an important role.
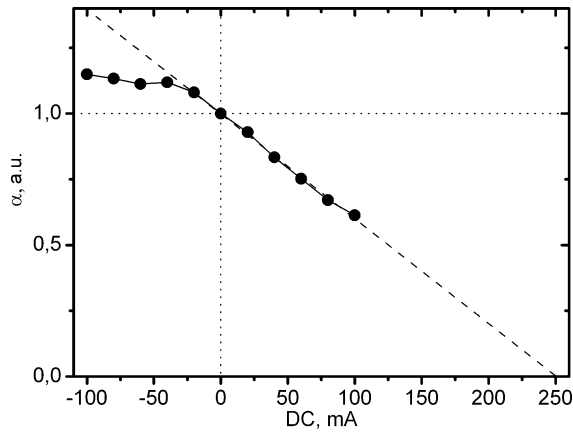
Fig. 10. Measured value of the damping constant as a function of the direct current. The dashed line is a result of a linear fit of the experimental data for positive values of the current.

ACKNOWLEDGMENT

REFERENCES

[1] S. Tehrani *et al.*, "Magnetoresistive random access memory using magnetic tunnel junctions," *Proc. IEEE*, vol. 91, no. 5, pp. 703–714, May 2003.

[2] A. Ney, C. Pampuch, R. Koch, and K. H. Ploog, "Programmable computing with a single magnetoresistive element," *Nature*, vol. 425, pp. 485–487, 2003.

[3] V. E. Demidov, U.-H. Hansen, and S. O. Demokritov, "Spin-wave eigenmodes of a saturated magnetic square at different precession angles," *Phys. Rev. Lett.*, vol. 98, p. 157 203, 2007.

[4] V. E. Demidov, S. O. Demokritov, G. Reiss, and K. Rott, "Effect of spin-polarized electric current on spin-wave radiation by spin-valve nanocontacts," *Appl. Phys. Lett.*, vol. 90, p. 172508, 2007.

[5] S. Choi, S.-K. Kim, V. E. Demidov, and S. O. Demokritov, "Double-contact spin-torque nano-oscillator with optimized spin-wave coupling: Micromagnetic modeling," *Appl. Phys. Lett.*, vol. 90, p. 083114, 2007.

[6] I. Neudecker *et al.*, "Spatially resolved dynamic eigenmode spectrum of Co rings," *Phys. Rev. Lett.*, vol. 96, p. 057207, 2006.

[7] J. Podbielski, F. Giesen, and D. Grundler, "Spin-wave interference in microscopic rings," *Phys. Rev. Lett.*, vol. 96, p. 167207, 2006.

[8] C. Mathieu *et al.*, "Lateral quantization of spin waves in micron size magnetic wires," *Phys. Rev. Lett.*, vol. 81, pp. 3968–3971, 1998.

[9] I. Neudecker *et al.*, "Modal spectrum of permalloy disks excited by in-plane magnetic fields," *Phys. Rev. B*, vol. 73, p. 134426, 2006.

[10] L. Le Guyader *et al.*, "Frequency analysis of the magnetization dynamics in thin ellipsoidal magnetic elements," *Phys. Rev. B*, vol. 73, p. 060402(R), 2006.

[11] M. Bolte, G. Meier, and C. Bayer, "Spin-wave eigenmodes of Landau domain patterns," *Phys. Rev. B*, vol. 73, p. 052406, 2006.

[12] M. Yan, G. Leaf, H. Kaper, R. Camley, and M. Grimsditch, "Spin-wave modes in a cobalt square vortex: Micromagnetic simulations," *Phys. Rev. B*, vol. 73, p. 014425, 2006.

[13] X. Zhu *et al.*, "Broadband spin dynamics of Permalloy rings in the circulation state," *Appl. Phys. Lett.*, vol. 86, p. 262502, 2005.

[14] V. E. Demidov, B. Hillebrands, S. O. Demokritov, M. Laufenberg, and P. P. Freitas, "Two-dimensional patterns of spin-wave radiation by rectangular spin-valve elements," *J. Appl. Phys.*, vol. 97, p. 10A717, 2005.

[15] J. C. Sankey *et al.*, "Mechanisms limiting the coherence time of spontaneous magnetic oscillations driven by dc spin-polarized currents," *Phys. Rev. B*, vol. 72, p. 224427, 2005.

[16] C. Bayer *et al.*, "Spin-wave excitations in finite rectangular elements of $Ni_{80}Fe_{20}$," *Phys. Rev. B*, vol. 72, p. 064427, 2005.

[17] J. P. Park and P. A. Crowell, "Interactions of spin waves with a magnetic vortex," *Phys. Rev. Lett.*, vol. 95, p. 167201, 2005.

[18] J. Raabe, C. Quitmann, C. H. Back, F. Nolting, S. Johnson, and C. Buehler, "Quantitative analysis of magnetic excitations in Landau flux-closure structures using synchrotron-radiation microscopy," *Phys. Rev. Lett.*, vol. 94, p. 217204, 2005.

[19] M. Buess, T. Haug, M. R. Scheinfein, and C. H. Back, "Micromagnetic dissipation, dispersion, and mode conversion in thin permalloy platelets," *Phys. Rev. Lett.*, vol. 94, p. 127205, 2005.

[20] K. Perzlmaier, M. Buess, C. H. Back, V. E. Demidov, B. Hillebrands, and S. O. Demokritov, "Spin-wave eigenmodes of permalloy squares with a closure domain structure," *Phys. Rev. Lett.*, vol. 94, p. 057202, 2005.

[21] G. Gubbiotti *et al.*, "Spin dynamics in thin nanometric elliptical Permalloy dots: A Brillouin light scattering investigation as a function of dot eccentricity," *Phys. Rev. B*, vol. 72, p. 184419, 2005.

[22] L. Giovannini *et al.*, "Spin excitations of nanometric cylindrical dots in vortex and saturated magnetic states," *Phys. Rev. B*, vol. 70, p. 172404, 2004.

[23] V. E. Demidov, S. O. Demokritov, B. Hillebrands, M. Laufenberg, and P. P. Freitas, "Radiation of spin waves by a single micrometer-sized magnetic element," *Appl. Phys, Lett.*, vol. 85, pp. 2866–2868, 2004.

[24] M. Grimsditch, G. K. Leaf, H. G. Kaper, D. A. Karpeev, and R. E. Camley, "Normal modes of spin excitations in magnetic nanoparticles," *Phys. Rev. B*, vol. 69, p. 174428, 2004.

[25] B. Van Waeyenberge *et al.*, "Magnetic vortex core reversal by excitation with short bursts of an alternating field," *Nature*, vol. 444, pp. 461–464, 2006.

[26] S. O. Demokritov, B. Hillebrands, and A. N. Slavin, "Brillouin light scattering studies of confined spin waves: linear and nonlinear confinement," *Phys. Rep.*, vol. 348, pp. 441–489, 2001.

[27] Y. Li *et al.*, "Micro-Brillouin scattering from a single isolated nanosphere," *Appl. Phys. Lett.*, vol. 88, p. 023112, 2006.

[28] L. D. Landau and E. M. Lifshitz, "On the theory of the dispersion of magnetic permeability in ferromagnetic bodies," *Phys. Z. d. Sowjetunion*, vol. 8, pp. 153–169, 1935.

[29] J. Jorzick *et al.*, "Spin wave wells in nonellipsoidal micrometer size magnetic elements," *Phys. Rev. Lett.*, vol. 88, p. 047204, 2002.

[30] R. W. Damon and J. R. Eshbach, "Magnetostatic modes of a ferromagnet slab," *J. Phys. Chem. Solids*, vol. 19, pp. 308–320, 1961.

[31] K. Y. Guslienko, S. O. Demokritov, B. Hillebrands, and A. N. Slavin, "Effective dipolar boundary conditions for dynamic magnetization in thin magnetic stripes," *Phys. Rev. B*, vol. 66, p. 132402, 2002.

[32] J. C. Slonczewski, "Excitation of spin waves by an electric current," *J. Magn. Magn. Mater.*, vol. 195, pp. L261–L268, 1999.

[33] S. I. Kiselev, J. C. Sankey, I. N. Krivorotov, N. C. Emley, R. J. Schoelkopf, R. A. Buhrman, and D. C. Ralph, "Microwave oscillations of a nanomagnet driven by a spin-polarized current," *Nature*, vol. 425, pp. 380–383, 2003.

[34] M. R. Pufall, W. H. Rippard, S. E. Russek, S. Kaka, and J. A. Katine, "Electrical measurement of spin-wave interactions of proximate spin transfer nanooscillators," *Phys. Rev. Lett.*, vol. 97, p. 087206, 2006.

[35] I. N. Krivorotov, N. C. Emley, J. C. Sankey, S. I. Kiselev, D. C. Ralph, and R. A. Buhrman, "Time-domain measurements of nanomagnet dynamics driven by spin-transfer torques," *Science*, vol. 307, pp. 228–231, 2005.

[36] F. B. Mancoff, N. D. Rizzo, B. N. Engel, and S. Tehrani, "Phase-locking in double-point-contact spin-transfer devices," *Nature*, vol. 437, pp. 393–395, 2005.

[37] A. Slavin and V. Tiberkevich, "Spin wave mode excited by spin-polarized current in a magnetic nanocontact is a standing self-localized wave bullet," *Phys. Rev. Lett.*, vol. 95, p. 237201, 2005.

[38] V. E. Demidov, S. O. Demokritov, G. Reiss, and K. Rott, "Effect of spin-polarized electric current on spin-wave radiation by spin-valve nano-contacts," *Appl. Phys. Lett.*, vol. 90, p. 172508, 2007.

[39] A. G. Gurevich and G. A. Melkov, *Magnetization Oscillations and Waves*. Boca Raton, FL: CRC, 1996.